Electronic Supplementary Material (ESI) for Catalysis Science & Technology.

Black TiO_{2-x} with Stable Surface Oxygen Vacancies as the Support of Efficient Gold Catalysts for Water-Gas Shift Reaction

Lei Li,*† Li Song,† Longfeng Zhu, Zheng Yan and Xuebo Cao*

College of Biological, Chemical Sciences and Engineering, Jiaxing University, Jiaxing, Zhejiang 314001, China

*Corresponding author, E-mail addresses: leili@mail.zjxu.edu.cn (L. Li), xbcao@mail.zjxu.edu.cn (X. Cao).

† These authors contributed equally.

Characterization

Powder XRD patterns of the as-synthesized samples were recorded by a PANalytical X' pert Pro diffractometer equipped with Cu-Kα (λ = 0.1541 nm) radiation (X'Celerator detector) operating at 40 kV and 40 mA with a scanning rate of 0.12 °/min. For Rietveld analysis, the XRD pattern of standard reference material (NIST 640A silicon), which is a material with no microstrain nor size broadening, was measured from 10° to 140° on the same instrument with the same experimental parameters. The patterns of the standard and experimental samples were fitted with a pseudo-Voigt function (PVF), which were carried out with X'pert highscore plus software. The actual Au loading in each catalyst was measured by ICP-OES using a Varian 710-ES analyzer. The morphology was examined by using field emission scanning electron microscopy (SEM, Hitachi S-4800) and transmission electron microscopy (TEM, JEM-2100). Gold cluster size distributions were measured using >200 particles for each sample to determine surface-averaged cluster diameters (d_{TEM}):[74]

$$d_{\mathrm{TEM}} = \frac{\sum n_i d_i^3}{\sum n_i d_i^2}$$

where n_i is the number of clusters with diameter d_i. Metal dispersions (D), defined as the fraction of

Au atoms exposed at cluster surfaces, and were estimated from d_{TEM}:

$$D = 6\frac{v_m/a_m}{d_{TEM}}$$

where v_m is the bulk atomic density of Au (16.49×10^{-3} nm^3) and a_m is the area occupied by an Au atom (8.75×10^{-2} nm^2) on a polycrystalline surface.[74]

Raman spectra were collected at room temperature on a Renishaw Invia Plus instrument using a semiconductor laser as an illumination source (532 nm). The electron paramagnetic resonance (EPR) spectra were collected using a Bruker EMX-8 spectrometer at room temperature. The settings were center field, 3510 G; microwave frequency, 9.859 GHz; and power, 10.02 mW. The X-ray photoelectron spectroscopy (XPS) measurements were performed on a VG ESCALAB 250 spectrophotometer with Al Ka radiation (1486.6 eV), operating at 15kV × 10 mA, in FAT mode (Fixed Analyser Transmission), with a pass energy of 30 eV for regions ROI and 100 eV for survey. The base pressure of the main chamber was kept at about 1×10^{-9} mbar. Each sample was first placed in a copper holder mounted on a sample-rod in the pretreatment chamber of the spectrometer, and it was then outgassed at 100 °C for 1 h before being transferred to the analysis chamber. A flood gun was always used for charge compensation. The spot size is 500 μm and each high-resolution spectrum was scanned for ten times with an energy step size of 0.05 eV. All binding energies (BE) were calibrated by using that of C 1 s (284.5 eV). The peaks obtained after a Shirley background subtraction were fitted to Lorentzian-Gaussian curves using a public software XPSPEAK version 4.1.

The BET surface area, pore volume and pore size distribution were measured by using nitrogen as adsorption gas at 77 K on a Micrometrics ASAP 2020 instrument. Temperature-programmed reduction (TPR) measurements were carried out on an AutoChem 2910 apparatus equipped with a thermal conductivity detector (TCD) for analysis. 50 mg of each sample was purged with high purity argon gas at 110 °C for 1 h, and cooled under the same gas flow to room temperature, finally reduced by H_2/Ar (H_2: 10 vol. %) with a flow of 30 mL/min in the temperature range of 50-600 °C at a heating rate of 10 °C/min. Diffuse reflectance spectroscopy (DRS) was measured on Agilent Cary 5000 UV-vis spectrophotometer in the range of 200-800 nm. The band gaps were estimated by extrapolating a

linear part of the plots to $(\alpha h\nu)^{0.5} = 0$. The photoluminescence (PL) spectra were obtained using Hitachi F-4500 fluorescence spectrophotometer with optical filter and the excitation wavelength at 300 nm. Mott-Schottky plots were derived from impedance-potential at a frequency of 10 KHz by a CHI 660D electrochemical station in the dark. 1M NaOH aqueous solution (pH = 13.6) was used as an electrolyte. Saturated calomel electrode (SCE) and Pt wire were used as reference and counter electrode, respectively.

Table S1. Physical properties of Au-TiO_2 and Au-TiO_{2-x} catalysts

Catalysts	Au loading (wt. %)[a]	Dispersion (%)[b]	TOF at 240 °C (s^{-1})	TOF at 200 °C (s^{-1})
Au-TiO_2-A	4.1	10	1.89	0.74
Au-TiO_{2-x}-A	4.0	9.7	3.49	1.43

a Measured by ICP-OES.

b Measured by TEM.

Table S2 Comparison of water-gas shift rates of Au-TiO_{2-x}-A catalysts with literature data.

Catalysts	Conditions	T (°C)	Ea (kJ/mol)	TOF (s^{-1})	Rate (μmol/g s)	Ref.
4 wt. %Au-TiO_{2-x}-A	6.25% CO, 50% H_2O, 43.75% N_2	200	45.4±2.2	1.43	14.4	This work
4 wt. %Au-TiO_{2-x}-A	6.25% CO, 50% H_2O, 43.75% N_2	240	45.4±2.2	3.49	41.1	This work
0.51 AuP25_UV_L	11% CO, 26% H_2O, 7% CO_2, 26% H_2 in He	200	45.2	0.2	6.3	*J. Am. Chem. Soc.* **2013**, 135, 3768-3771.
2.3 wt.% Au/TiO_2	7% CO, 11% H_2O, 9% CO_2, 37% H_2, balance He	120	56 ± 3		0.011 (mol H_2) (mol Au)$^{-1}$ s^{-1}	*J. Catal.* **2012**, 289, 171-178.
Au-TiO_2	6.8% CO, 21.9% H_2O,	120	45-60		0.1 (mol H_2)	*J. Am. Chem. Soc.*

	8.5% CO_2, 37.4% H_2, balance Ar				(mol Au) $^{-1}$ s^{-1}	**2012**, 134, 4700-4708.
Au/TiO_2 (DP, 3.4%)	1% CO, 2% H_2O, He (balance)	100	46	0.00079	0.1	*Chem. Commun.* **1997**, 271-272.
1.5 wt.% $Au-TiO_2$	4.76%CO, 10.06% CO_2, 28.46% H_2, 35.38% H_2O, 21.34% N_2	300		0.18		*Int. J. Hydrogen Energ.* **2016**, 41, 4670-4681.
Au/TiO_2-Ni 1	5% CO, 10%H_2O in He balance	300		0.0053 h^{-1}		*RSC Adv.* **2014**, 4, 4308-4316.
0.5 wt.%$Pt/Na-TiO_2$	3% CO and 10% H_2O (balance He)	250	71	1.58	38.4	*J. Catal.* **2009**, 267, 57-66.
$Pt/Na-TiO_2$	2.83% CO, 5.66% H_2O, 37.74% H_2, 53.77% He	250	80	1.39	20	*J. Catal.* **2011**, 278, 123-132.
0.5% $Pt/CaO-TiO_2$	3% CO and 10% H_2O (balance He)	220	72.8	0.38	9.52	*Appl. Catal. B-Environ.* **2011**, 101, 738-746.
30Na:Pt/Al_2O_3	7% CO, 11% H_2O, 9% CO_2, 37% H_2, 10% Ar, balance He	250	77	0.35	7.6(mol H_2) (mol Pt) $^{-1}$ s^{-1}	*J. Catal.* **2016**, 339, 163-172.
$Pt/Ce_{0.75}Zr_{0.25}O_2$	5% H_2, 15% CO, 5% CO_2, 20% H_2O, and balance N_2 plus 50 ppm of H_2S	200	47 ± 6	0.0337		*J. Catal.* **2016**, 341, 1-12.
3.7% Pt/Mo_2C	11% CO, 21% H_2O, 6% CO_2, 43% H_2, 19% N_2	240	49 ± 4	0.72	1.3(mol H_2) (mol Pt) $^{-1}$ s^{-1}	*J. Catal.* **2015**, 330, 280-287.
1.5% Pt/Mo_2C	7% CO, 8.5% CO_2, 22% H_2O, 37.5% H_2, balance Ar	120	48		1.8	*J. Catal.* **2015**, 331, 162-171.
0.01 wt.% Ir/FeO_x	2% CO, 10% H_2O in He	300	50	2.31		*J. Am. Chem. Soc.* **2013**, 135, 15314-15317.
$5Ni5Cu/CeO_2$	7% CO, 22% H_2O, 10% CO_2, 20% H_2, balance He	350	41.3	0.013		*J. Catal.* **2014**, 314, 32-46.

1

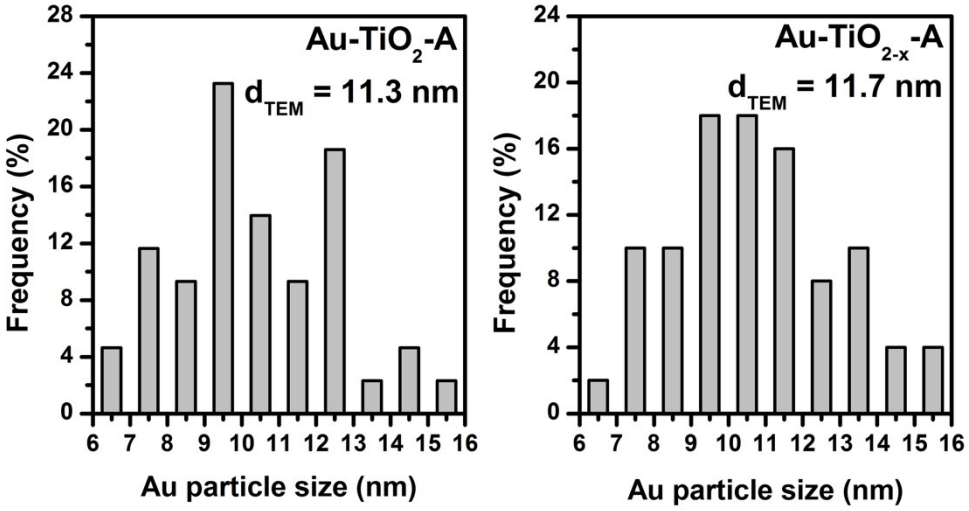

Figure S1. Surface-averaged Au cluster diameters (d_{TEM}) and cluster diameter distributions of Au-TiO_2 and Au-TiO_{2-x} catalysts

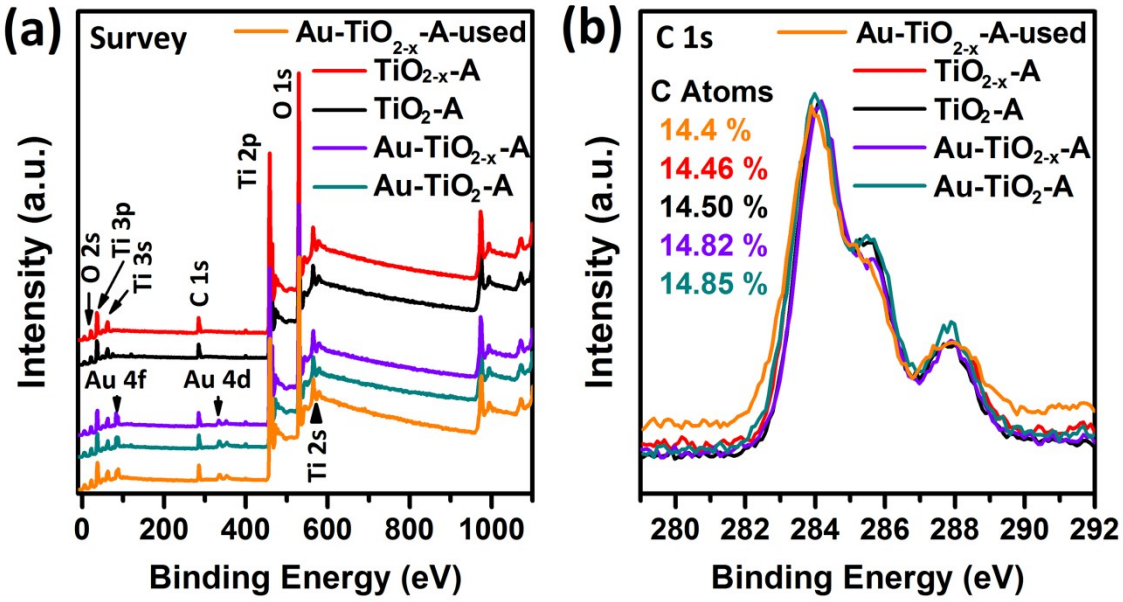

Figure S2. XPS spectra of various TiO_2 supports and Au-TiO_2 catalysts.

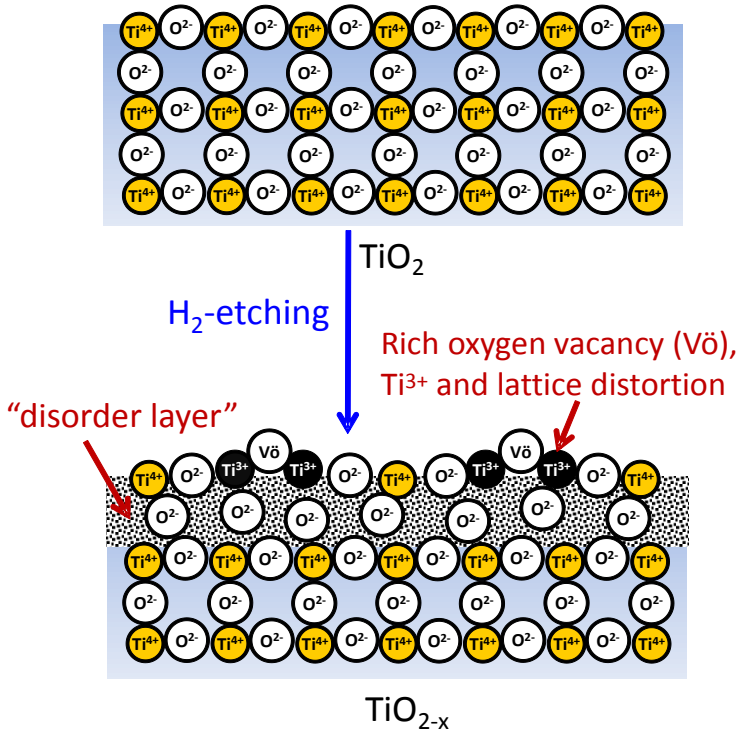

Figure S3. Schematic structure of white and black TiO_2.

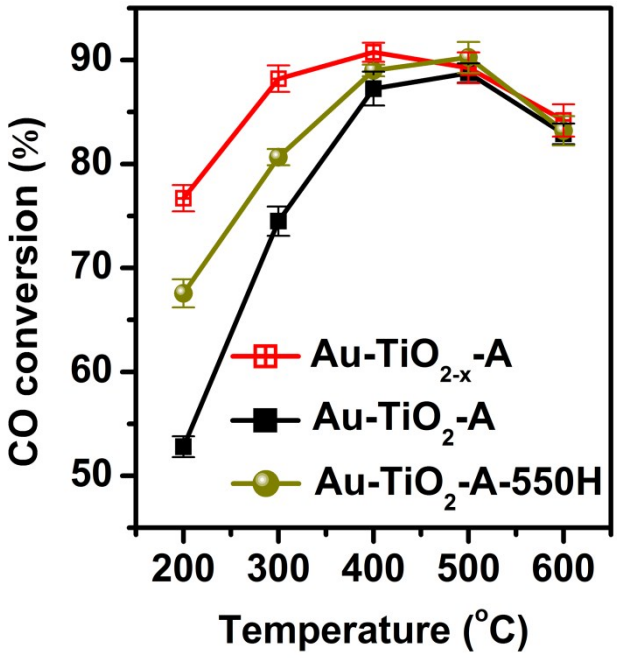

Figure S4.The CO conversions of Au-TiO_2-550H compared with Au-TiO_2-A and Au-TiO_{2-x}-A catalysts.

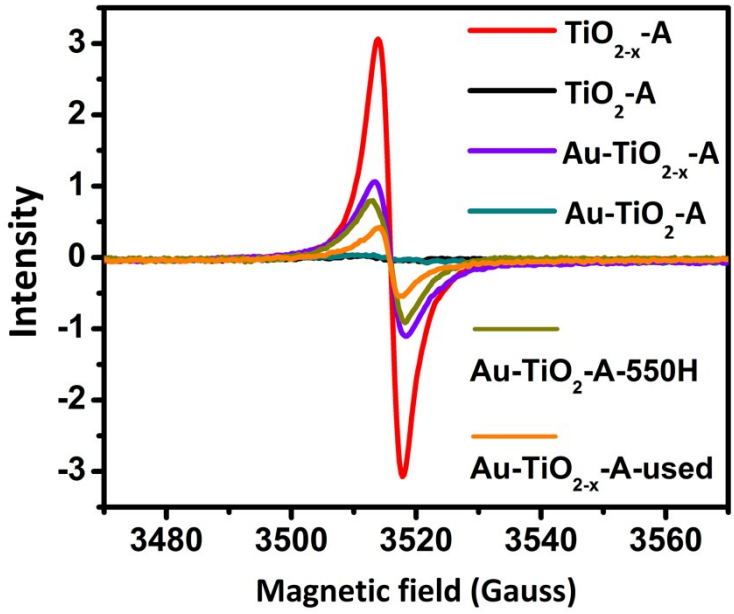

Figure S5. EPR spectra of Au-TiO_2-550H compared with Au-TiO_2-A and Au-TiO_{2-x}-A catalysts.

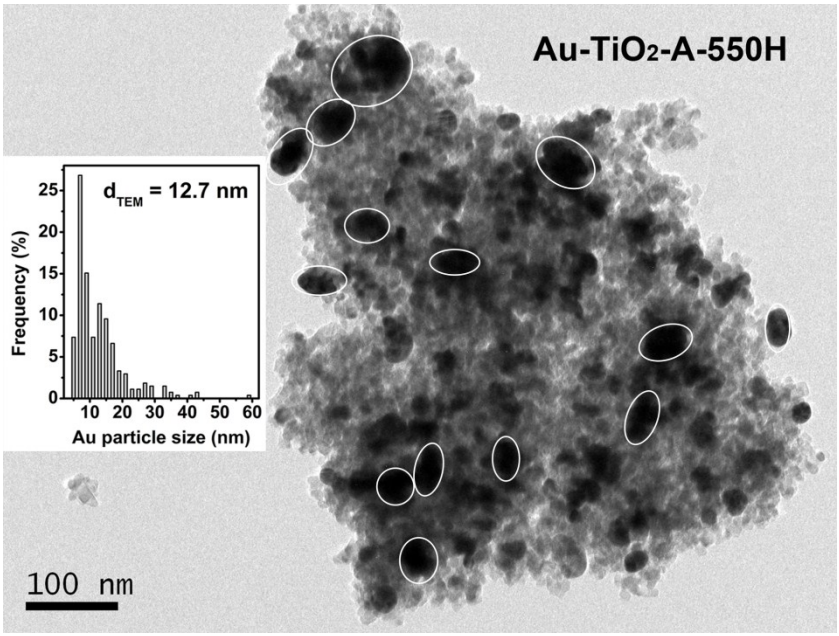

Figure S6. TEM images, surface-averaged Au cluster diameters (d_{TEM}) and cluster diameter distributions of Au-TiO_2-A-550H catalysts

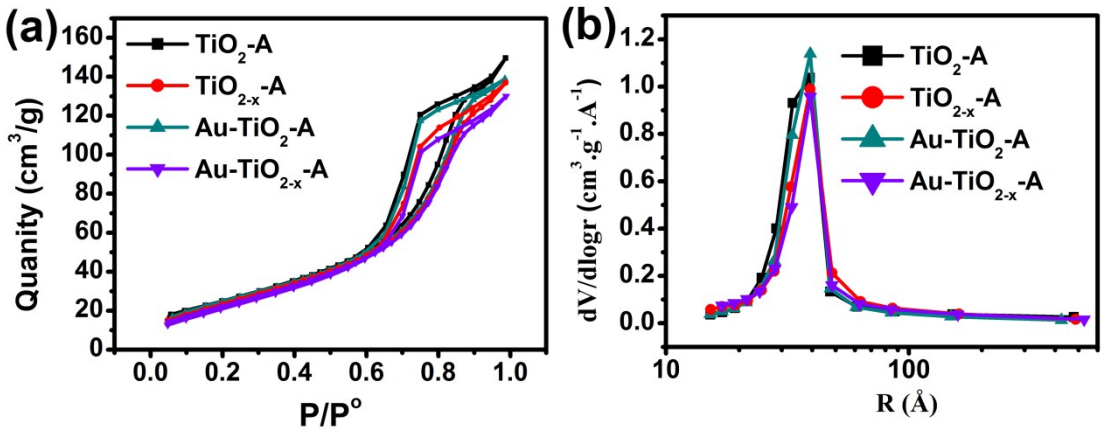

Figure S7. Adsorption-desorption isotherms (a) and pore size distribution (b) of various TiO_2 supports and Au-TiO_2 catalysts.

By comparison, hydrogen-etching technology has hardly obvious effect on adsorption-desorption isotherms and pore size distribution of TiO_2 supports and Au-TiO_2 catalysts.

Table S3 Texture properties of various TiO_2 supports and Au-TiO_2 catalysts.

Sample	S_{BET} (m^2/g)	Total pore volume (cm^3/g)	Average pore radius (Å)
TiO_2-A	95.1	0.231	48.6
TiO_{2-x}-A	92.7	0.212	45.7
Au-TiO_2-A	96.1	0.215	44.8
Au-TiO_{2-x}-A	89.4	0.201	45.0

Finally, hydrogen-etching technology also has little effect on S_{BET}, total pore volume and average pore radius of TiO_2 supports and Au-TiO_2 catalysts.

Therefore, the differences in WGS catalytic activities should not be attributed to their difference of texture properties but surface structure and optoelectric properties.

Calculation on heat and mass transfer limitation

We calculated the heat and mass transfer limitation, according to the literatures (*Mass and heat transfer in catalytic reactions, Catalysis Today, 1999, 52, 147-152,* and *Tests for Transport limitations in Experimental Catalytic Reactors,*

Ind. Eng. Chern. Process Des. Develop., 1971, 10(4), 541-547.). The fundamental data are from *CRC Handbook of Chemistry and Physics* (95th Edition). The detailed calculations of Au-TiO_{2-x}-A catalyst at 473.15 K were presented as follows:

To ensure that kinetic data obtained in an experimental reactor reflect only chemical events, temperature and concentration gradients must be virtually eliminated from three domains:

Intraparticle within individual catalyst particles;

Interphase between the external surface of the particles and fluid adjacent to them;

Interparticle between the local fluid regions or catalyst particles.

The objective has been to calculate an effectiveness factor, η, defined as the ratio of the actual rate to that which would occur if the temperature and concentration were constant throughout the catalyst particle. To eliminate temperature and concentration gradients, it is necessary to ensure $\eta \geq 0.95$.

The calculated results suggest that external diffusion limitation, internal diffusion limitation, interphase heat transfer limitation and interparticle heat transfer limitation have been eliminated.

1. Eliminating mass transfer limitation

To eliminate mass transfer limitation, we have kept low CO conversion (below 12%) by decreasing the catalyst weight and particle diameter (100 - 120 mesh) and adjusting the flow rate of feed gas.

1.1 Eliminating external diffusion limitation

The criterion can be expressed in terms of Damköhler number:

$$\ddot{R}\, r_p / C_b\, k_c < 0.15 / n$$

where $\ddot{R}$ ($mol \cdot s^{-1} \cdot cm^{-3}$) is the observed reaction rate per unit particle volume, r_p (cm) is the radius of the particle (100 mesh / 2 = 0.0075 cm), C_b (5.6×10^{-6} $mol \cdot cm^{-3}$) is the bulk fluid concentration, k_c ($cm \cdot s^{-1}$) is mass transfer coefficient between gas and particle, and n is the reaction order. Hereinto, k_c was calculated as follows:

Reynolds numbers ($Re = D_p \rho u_s / \mu$):

$$Re = \frac{0.015 \times 0.72 \times 10^3 \times 8}{24.7 \times 10^{-6}} = 3.5$$

where D_p (cm) is the catalyst particle diameter (100 mesh = 0.015 cm), ρ (0.72×10^{-3} g·cm^{-3}) is the density of CO, u_s (cm·s^{-1}) is the superficial flow rate of the fluid (8 cm·s^{-1}). μ (24.7×10^{-6} Pa·s) is the viscosity of CO.

For gaseous reactants, 3 < Re < 2000 and 0.416 < ϵ < 0.788,

$$j_D \epsilon = 0.357\, Re^{-0.359} = 0.228$$

$$j_D = 0.228 / 0.5 = 0.455$$

where ϵ (0.5) is the interparticle void fraction of the bed of particles.

$$j_D = \frac{k_c}{u_s}\left(\frac{\mu}{\rho D}\right)^{0.67} = \frac{k_c}{8}\left(\frac{24.7 \times 10^{-6}}{0.72 \times 10^{-3} \times 0.491}\right)^{0.67}$$

where D (0.491 cm^{-2}·s^{-1}) the diffusion coefficient of the reactant (CO in N_2).

$$k_c = 21.6 \text{ cm·s}^{-1}$$

$$\frac{\ddot{\mathrm{R}} r_p}{C_b k_c} = \frac{1.1 \times 10^{-4} \times 0.0075}{21.6 \times 5.6 \times 10^{-6}} = 0.007 < \frac{0.15}{n} = \frac{0.15}{1}$$

where n = 1 (first-order reaction).

Therefore, the external diffusion had been eliminated.

1.2 Eliminating internal diffusion

The criterion requires:

$$\ddot{\mathrm{R}}\, r_p^2 / C_s D_e < 1$$

where C_s (5.25×10^{-6} mol·cm^{-3}) is the reactant concentration at the external surface of particle, D_e (cm^2·s^{-1}) is effective diffusion coefficient. Hereinto, D_e was calculated as follows:

$$1 / D_e = 1 / D_{b,e} + 1 / D_{k,e}$$

where $D_{b,e}$ and $D_{k,e}$ are the effective diffusion coefficients for bulk and Knudsen diffusion,

respectively. They can be calculated by the following equations:

$$D_{b,e} = D_b\theta/\tau = 0.491\times0.5/4=0.0614$$

$$D_{k,e} = 1.94\times10^4\frac{\theta^2}{\tau S_g\rho_P}\sqrt{\frac{T}{M}} = 1.94\times10^4\frac{0.5^2}{4\times89.4\times10^4\times4}\sqrt{\frac{473.15}{28}} = 0.0014$$

where D_b ($cm^2\cdot s^{-1}$) is the bulk diffusion coefficient, θ the internal void fraction of the solid particle, τ the tortuosity factor of the pores, S_g ($cm^2\cdot g^{-1}$) the specific surface area of the catalyst, ρ_p ($g\cdot cm^{-3}$) the particle density, T (K) the reaction temperature and M ($g\cdot mol^{-1}$) the molecular mass of the diffusing species. A value of ca. 0.5 and of ca. 4 can be attributed to θ and τ, respectively.

$$D_e = 0.0014$$

$$\frac{\hat{R}\,r_P^{\,2}}{C_sD_e} = \frac{1.1\times10^{-4}\times0.0075^2}{5.25\times10^{-6}\times0.0014} = 0.8 < 1$$

Therefore, the internal diffusion had been eliminated.

2. Eliminating heat transfer limitation

To eliminate heat transfer limitation, we have diluted the catalyst with low surface area quartz sands and used the tubular reactor with small diameter (7mm). The magnitudes of the heat transport resistances in experimental reactors are generally in the order: interparticle > interphase > intraparticle. The effect of temperature distribution within a catalyst particle is usually very less and can be negligible.

2.1. Eliminating interphase heat transfer limitation

The criterion requires:

$$\left|\frac{-\Delta H\hat{R}r_P}{hT_b}\right| < 0.15\frac{RT_b}{E}$$

where ΔH (41.7×238.9 $cal\cdot mol^{-1}$) is heat of chemical reaction, T_b is the temperature of the bulk fluid, and h ($cal\cdot s^{-1}\cdot cm^{-2}\cdot K^{-1}$) is the heat transfer coefficient, R (8.314×0.2389 $cal\cdot mol^{-1}\cdot K^{-1}$) is gas constant, E (45.4×238.9 $cal\cdot mol^{-1}$) is intrinsic activation energy. Hereinto, h was calculated as follows:

$$j_H = \frac{h}{c_p \rho u_s}\left(\frac{c_p \mu}{k}\right)^{0.67} = \frac{h}{1.04 \times 0.72 \times 10^{-3} \times 8}\left(\frac{1.04 \times 24.7 \times 10^{-6}}{3.73}\right)^{0.67}$$

where C_p (1.04 J·g^{-1}·K^{-1}) is the heat capacity of CO, k (3.73 W·cm^{-1}·K^{-1}) is the thermal conductivity of CO.

$$j_H = 1.08\, j_D = 0.4914$$

$$h = 8.5 \text{ J·s}^{-1}\text{·cm}^{-2}\text{·K}^{-1} = 2.03 \text{ cal·s}^{-1}\text{·cm}^{-2}\text{·K}^{-1}$$

$$\left|\frac{-\Delta H \ddot{R} r_P}{h T_b}\right| = \left|\frac{41.7 \times 238.9 \times 1.1 \times 10^{-4} \times 0.0075}{2.03 \times 473.15}\right| = 8 \times 10^{-6} < 0.15\frac{RT_b}{E} = 0.15 \times 0.013$$

Therefore, interphase heat transfer limitation had been eliminated.

2.2. Eliminating interparticle heat transfer limitation

The criterion requires:

$$\left|\frac{-\Delta H \ddot{R}_b {R_o}^2}{k_e T_w}\right| < 0.4\frac{RT_w}{E}$$

where k_e (0.26 cal·s^{-1}·cm^{-1}·K^{-1}) is the effective thermal conductivity of the bed (quartz sands), $\ddot{R}_b$ (1.6×10^{-6} mol·s^{-1}·cm^{-3}) is reaction rate per unit bed volume, R_o (0.35 cm) is radius of tubular reactor. T_w is absolute temperature of the reactor wall.

$$\left|\frac{-\Delta H \ddot{R}_b {R_o}^2}{k_e T_w}\right| = \left|\frac{41.7 \times 238.9 \times 1.6 \times 10^{-6} \times 0.35^2}{0.26 \times 473.15}\right| = 1.6 \times 10^{-5} < 0.4\frac{RT_w}{E} = 0.4 \times 0.035$$

Therefore, interparticle heat transfer limitation had been eliminated.